Continental Shelf Research 35 (2012) 117–128

Contents lists available at SciVerse ScienceDirect

Continental Shelf Research

journal homepage: www.elsevier.com/locate/csr

Research papers

Influence of suspended particle concentration, composition and size on the variability of inherent optical properties of the Southern North Sea

R. Astoreca [a,*], D. Doxaran [b], K. Ruddick [c], V. Rousseau [a], C. Lancelot [a]

[a] Ecologie des Systèmes Aquatiques (ESA), Faculté des Sciences, Université Libre de Bruxelles, Campus Plaine-CP 221, Boulevard du Triomphe, B-1050 Brussels, Belgium
[b] Université Pierre et Marie Curie, Laboratoire d'Océanographie de Villefranche, Centre National de la Recherche Scientifique, Villefranche-sur-Mer, France
[c] Management Unit of the North Sea Mathematical Models (MUMM), Royal Belgian Institute for Natural Sciences, Brussels, Belgium

ARTICLE INFO

Article history:
Received 20 September 2010
Received in revised form
1 December 2011
Accepted 9 January 2012
Available online 17 January 2012

Keywords:
Inherent optical properties
Coastal-offshore transect
Organic/inorganic particles
Chlorophyll *a*
Total suspended matter
Southern North Sea

ABSTRACT

Suspended particles play an important role in coastal waters by controlling to a large extent the variability of the water inherent optical properties (IOPs). In this study, focused on the complex waters of the Southern North Sea, the relationships between the concentration, composition and size of suspended particles and their optical properties (light absorption, and attenuation in the visible and near-infrared spectral regions) are investigated. Over a one-year period, field measurements were carried out along regular transects from the Belgian to the English coasts to cover a wide gradient of water masses. Results show that the area can be divided into three geographical zones, each one having specific biogeochemical and optical properties: Scheldt coastal zone (SCZ), Middle of the Southern North Sea (MSNS) and Thames coastal zone (TCZ). Concentrations of organic (inorganic) particles were always higher in the SCZ (TCZ). The MSNS was characterized by a high proportion of organic particles in low concentration. The spectral shape of particle attenuation reveals a wide range from negative to positive slopes. Particle size distributions reveal a power-law shape along the coasts (especially in the TCZ) and a bimodal distribution in the MSNS notably during the spring phytoplankton bloom. This bimodal size distribution and more precisely a size peak around 7 μm results in an unexpected negative spectral slope of the particle attenuation coefficient. Variations in the particulate mass-specific IOPs between the three regions were observed to predominate over seasonal variations. The implications in terms of inversion of IOPs into biogeochemical parameters, such as chlorophyll *a* and total suspended matter, in coastal waters are discussed.

1. Introduction

The color of natural waters depends on the concentration and type of suspended particles and dissolved material it contains. Several types of marine waters can be distinguished from 'clear' waters with low concentration of particles, usually in open ocean environments, to 'turbid' waters where the concentration of particles is high, usually in coastal and estuarine environments.

Suspended organic and inorganic particles have various origins in coastal systems: direct inputs from rivers, sediment resuspension by tidal motions or in situ via primary production (Chester, 2000; Falkowski, 1994). Their presence in the water column alters the penetration of solar light and thus influences light-related processes such as photosynthesis (Williams et al., 2002).

Particulate light absorption (a_p), scattering (b_p) and attenuation (c_p) coefficients depend on the composition, size and concentration of marine particles: they are inherent optical properties (IOPs) of waters that contribute to ocean color by modifying the reflectance signal (Kirk, 1994). Therefore, information on the concentration, composition and size of marine particles and on particle dynamics can potentially be extracted from IOPs and ocean color measurements.

Also, a prior knowledge of the specific IOPs (i.e. IOPs per unit of suspended particle concentration) is needed for the retrieval of biogeochemical parameters from remote sensing reflectance. In the open ocean, the particulate light absorption has been found to covary with chlorophyll *a* (CHL) and total suspended matter (TSM) concentrations (Bricaud et al., 1998). Particulate scattering has been found to be directly related to TSM concentration, but this relationship varies from oceanic to coastal areas (Babin et al., 2003a). These parameterizations have been useful for the remote sensing of parameters linked to water particle load, i.e. CHL and TSM concentrations, at a regional scale (Schiller and Doerffer, 1999). However, the extent to which these relationships are valid

* Corresponding author. Tel.: +32 26505924; fax: +32 26505993.
E-mail addresses: rastorec@ulb.ac.be (R. Astoreca), doxaran@obs-vlfr.fr (D. Doxaran), k.ruddick@mumm.ac.be (K. Ruddick), vrousso@ulb.ac.be (V. Rousseau), lancelot@ulb.ac.be (C. Lancelot).

0278-4343/$ - see front matter © 2012 Elsevier Ltd. All rights reserved.
doi:10.1016/j.csr.2012.01.007

at a larger spatial scale is unknown because of the variability of the mass-specific IOPs. Regional characterization of the IOPs is thus a crucial step in the development of algorithms for the inversion of biogeochemical parameters in coastal waters. This was pointed out, for example, by Eleveld et al. (2008) for the Southern North Sea who highlighted that their TSM retrieval algorithm, created with Dutch and Belgian IOPs data, must be used with care in English coastal waters due to differences in mass-specific IOPs. A caution was also given by Babin et al. (2003b) on their general relationship between non-algal particles (NAP) absorption and TSM since considerable variability of this relationship was also observed.

Recently, the spectral variations of IOPs, i.e. their spectral shapes, were shown to provide information on particle composition and size. The spectral shape of a_p has been related to pigment composition in oceanic waters where the spectra of a_p resemble that of phytoplankton absorption due to the low NAP contribution (Eisner et al., 2003). The spectral variations of the particulate single scattering albedo, has been used to distinguish mineral and algal composition of a water sample (Babin et al., 2003a). Furthermore, the shape of the particle size distribution has been found to be related to the spectral slope of the attenuation and/or scattering coefficients in coastal waters (Boss et al., 2001a, 2001b; Doxaran et al., 2007, 2009).

The Southern North Sea is a shallow area where strong tidal currents and energetic wave regimes favor the resuspension of bottom sediments resulting in high concentrations of TSM (Fettweis and Van Den Eynde, 2003). This area is characterized by seasonal variations of IOPs and biogeochemical parameters (Astoreca et al., 2006, 2009a, 2009b). In April each year an important phytoplankton bloom extends all over the area (Lancelot et al., 1987; Lancelot, 1995) resulting in maximum CHL concentrations up to 100 mg m^{-3} in nearshore stations. In addition to phytoplankton, high concentrations of mineral particles are systematically observed in the coastal waters.

A detailed parameterization of the IOPs and specific IOPs is required in the Southern North Sea for accurate inversion of biogeochemical parameters from field optical measurements and ocean color satellite data. The impediment is the scarcity of data on particle composition and size variations in this area.

In this study, field biogeochemical and optical measurements carried out during several cruises along a seasonal cycle in 2009 are used to characterize the variability of the (mass-specific) IOPs of suspended particles in the Southern North Sea in relationship with particle concentration, composition and size distribution. The overall objective is to determine whether the Southern North Sea can be considered as a homogenous region with respect to mass-specific IOPs or, on the contrary, if different optical regions can be identified thus constraining the use of regional sets of specific IOPs for remote sensing reflectance inversion of biogeochemical parameters.

2. Data and methods

2.1. Field study area and sampling stations

Field measurements were carried out in order to characterize the spatial and seasonal variability of biogeochemical and optical properties of suspended particles. The study area is the Southern North Sea where a transect was performed from the Belgian to the English coasts respectively influenced by the Scheldt and Thames river discharges (Fig. 1). This transect covers a wide range of salinities from low salinity estuarine coastal waters to offshore Atlantic waters (salinity ~35) in the middle of the Southern North Sea (MSNS) (Fig. 2). The water depth along this transect

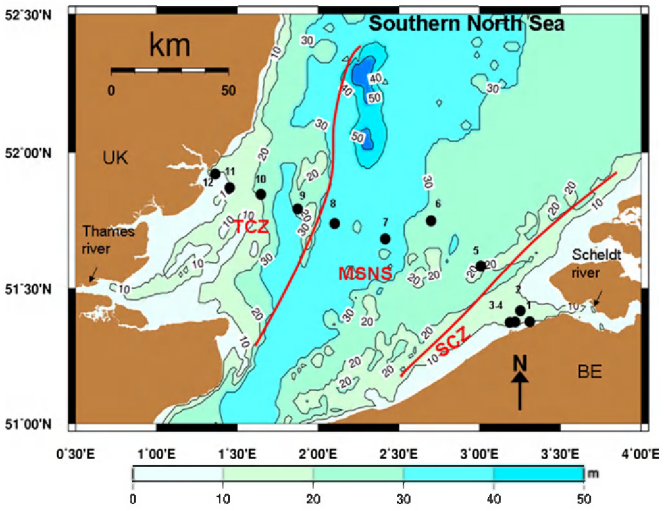

Fig. 1. Study area and sampling stations (stations are numbered from 1 to 12 from the SCZ to the TCZ). The red lines distinguish the three geographical zones identified from salinity and depth transects (Fig. 2). The Scheldt and Thames river discharges are shown with arrows. The color scale shows the bathymetry. (For interpretation of the references to colour in this figure legend, the reader is referred to the web version of this article.)

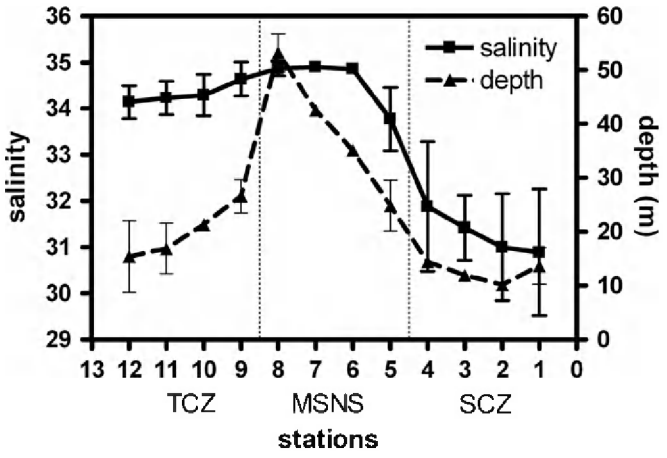

Fig. 2. Variability of salinity and water depth along the SCZ–TCZ transect for the three 2009 cruises. Inter-cruises variability is shown as standard deviation bars.

varies from 5 to 25 m nearshore up to 55 m in the MSNS (Fig. 2). Based on the salinity and depth gradient (Fig. 2), three distinct zones were identified in the Southern North Sea: the Scheldt coastal zone (SCZ) with minimum salinity and depth up to 20 km from the coast; the MSNS with maximum salinity and depth; and the Thames coastal zone (TCZ) with high salinity and moderate depths up to 40 km from the coast.

Three cruises were conducted in 2009, respectively in spring (20–24/04), summer (16–19/06) and late summer (15–18/09). Twelve stations were sampled during each cruise along the SCZ–TCZ transect (Fig. 1). An existing dataset comprising biogeochemical and optical data available for 2005–2008 is also used in our study to globally assess the variability of these parameters in this area. This set includes data gained during three cruises performed each year (April, June/July, September) in the Belgian, Dutch and English coastal zones and includes other stations than the ones sampled in 2009.

At each station a bottle of 20 L was rinsed twice and filled with sub-surface water collected using a Niskin bottle (or an

oceanographic bucket during the April cruise to avoid *P. globosa* colony disruption), for the determination of biogeochemical (CHL and TSM concentrations; organic fraction of TSM, OSM/TSM; inorganic fraction of TSM, ISM/TSM) and optical properties (colored dissolved organic matter absorption, a_{CDOM} in m^{-1}; absorption and attenuation coefficients in m^{-1}; particle size distributions).

2.2. Biogeochemical measurements

The concentration of CHL (in mg m^{-3}) was determined following the spectrophotometric method of Lorenzen and Jeffrey (1980). Between 0.2 and 3.6 L of surface water were filtered through Whatman GF/F glass-fiber filters (either 25 or 47 mm) and then stored at −20 °C until analysis (not more than one week later). Pigment extraction was performed using 90% acetone, filters were grounded and centrifuged, and absorbance maxima were measured before and after acidification with 1 N HCl. The CHL concentration was calculated using the equations in Lorenzen and Jeffrey (1980).

TSM concentration (in g m^{-3}) was determined by gravimetry. Between 0.15 and 1 L of surface water were filtered through Nuclepore 0.6 μm pore-size pre-weighed membranes and stored at −20 °C. Membranes were then dried 12 h at 80 °C and re-weighed to obtain the concentration of TSM. Membranes were re-weighed after burning for 5 h at 450 °C to measure inorganic suspended matter (ISM) concentration. The organic fraction of TSM (OSM/TSM) was calculated as: (TSM–ISM)/TSM and the inorganic fraction as: ISM/TSM.

2.3. Optical measurements

Colored dissolved organic matter absorption (a_{CDOM}) was determined by filtration of 100 ml of seawater through a 0.2 μm Nuclepore PC membrane previously rinsed with Milli-Q water, this volume was used to rinse the glassware and then discarded. A second volume of 100 ml seawater was filtered and kept in an amber bottle at 4 °C until analysis. All glassware was previously combusted at 450 °C for 4 h. The a_{CDOM} was measured, at room temperature, between 400 and 750 nm with a double beam spectrophotometer (Perkin Elmer Lambda 650) using a 10 cm cuvette. The average optical density between 683 and 687 nm was subtracted from the data as a baseline correction (Astoreca et al., 2009b).

Total non-water absorption $a(\lambda)$ and beam attenuation $c(\lambda)$ coefficients, both in m^{-1}, were measured with an ac-9 attenuation and absorption meter (WetLabs, Inc) which measures at 412, 440, 488, 510, 555, 630, 650, 676 and 715 nm along a 25 cm path length.

The ac-9 was placed vertically on a bench. A water calibration using fresh Milli-Q water was performed every day. Surface seawater was passed through the absorption and attenuation tubes of the ac-9. Data were recorded during 2 min, and then the median was taken over 0.5-minute noise-free data. The raw data were corrected according to Pegau et al. (1997) for temperature and salinity both measured with a Seabird Thermosalinometer SBE-21. Absorption measurements were corrected for residual scattering using the proportional method (Zaneveld et al., 1994) using 715 nm as the near-infrared reference wavelength.

The particle attenuation coefficient $c_p(\lambda)$ was obtained by subtracting $a_{CDOM}(\lambda)$ from $c(\lambda)$.

The TSM-specific attenuation $c_p^*(\lambda)$ coefficient, in $m^2\ g^{-1}$, was computed by normalizing $c_p(\lambda)$ to TSM.

For comparison, a second and shorter (10 cm path length) ac-9 having four common wavelengths (440, 555, 630, 715 nm) was used to also measure on a bench the optical properties of each collected water sample. The coefficient of determination, R^2, obtained when comparing the attenuation coefficients measured by the two sensors at 440, 555, 630 and 715 nm, was systematically higher than 0.98. The mean value and standard deviation of the differences between these two instruments were between 0.09 and 0.22 and between 1.06 and 1.27 m^{-1}, respectively. The corresponding R^2 obtained when comparing the measured absorption coefficients at 440, 555 and 630 nm was higher than 0.97. The mean value and standard deviation of the differences between instruments were between 0.14 and 0.38 and between 0.14 and 0.39 m^{-1}, respectively. Note that Leymarie et al. (2010) showed that the influence of multiple scattering as a function of the tube length (10 or 25 cm) in the determination of the absorption coefficient is low, between 5 and 10%, which is comparable to the magnitude of the uncertainties due to pure water calibration of the sensors.

Particle absorption, a_p in m^{-1}, was also measured on particles retained on glass–fiber filters using a spectrophotometer following the Transmittance–Reflectance method of Tassan and Ferrari (1995, 2002). Transmittance and reflectance of a GF/F filter containing the sample were measured between 400 and 750 nm with a Perkin Elmer Lambda 650 spectrophotometer equipped with a 15 cm-integrating sphere. Pathlength amplification was corrected for using an algorithm already validated for several phytoplankton species and detrital particles (Tassan and Ferrari, 1998). The filter was bleached with a solution of sodium hypochlorite (0.13% active chlorine) to obtain the absorbance spectrum of non-algal particles (NAP) including depigmented algal cells retained on the filter $OD_{NAP}(\lambda)$ (Ferrari and Tassan, 1999). Absorbance values at each wavelength were converted into absorption coefficients as

$$a_{P/NAP}(\lambda) = 2.303 * OD_{P/NAP}(\lambda)/X \quad (1)$$

where X is the ratio of filtered volume to the filter clearance area. Absorption was corrected for scattering in the near-infrared by subtracting the average value between 746 and 750 nm from the final absorption values as most turbid stations showed residual scattering in the near- infrared.

The phytoplankton absorption coefficient, $a_{ph}(\lambda)$ in m^{-1}, was computed as the difference between $a_p(\lambda)$ and $a_{NAP}(\lambda)$. The CHL-specific phytoplankton absorption coefficient, a_{ph}^* in $m^2\ mg^{-1}$, was calculated as the phytoplankton absorption coefficient normalized to CHL. The TSM-specific NAP absorption coefficient, a_{NAP}^* in $m^2\ g^{-1}$, was calculated as the a_{NAP} normalized to TSM.

The particle absorption coefficient measured with the spectrophotometer was compared with that measured with the ac-9 (a-a_{CDOM}). The R^2 coefficient for this comparison at 440, 488, 555 and 676 nm was higher than 0.95. The mean value and standard deviation of the differences between these two instruments were between 0.02 and 0.10 and between 0.04 and 0.22 m^{-1}, respectively.

Assuming suspended particles to be spherical, homogenous and non-absorbing with a size distribution spanning from 0 to infinity according to a power law distribution, the spectral variations of the particulate attenuation coefficient, c_p, can be modeled using a power-law function (Morel, 1973). The measured $c_p(\lambda)$ spectra were therefore fitted to the following function:

$$c_p(\lambda) = c_p(715) * (\lambda/715)^{\gamma cp} \quad (2)$$

where γ_{cp} is the c_p spectral slope. The γ_{cp} spectral slopes were calculated from 555 to 715 nm using a least-square fit. When compared to the spectral slopes calculated from 440 to 715 nm, they were found to be similar (slope = 1.02, intercept = −0.070, $R^2 = 0.84$, F-ratio = 1223.8, $p < 0.0001$).

Particle size distributions (PSDs) were estimated from field measurements of the volume scattering function performed using

a LISST-100X Type-C particle size analyzer (Sequoia, Inc). Sub-surface data (0–0.5 m) were averaged to be related to the measured IOPs and biogeochemical parameters. Prior to each LISST deployment, a background measurement was carried out using 0.2 μm-filtered seawater. Particle size and volume concentrations were processed using the LISST-SOP software. Particle number concentrations were obtained by dividing the volume concentration measured for each size bin by the volume of a sphere of the same diameter to obtain numbers of equivalent spherical diameter for each size bin. The size distribution of particles for each sample was obtained in 32 logarithmically spaced size classes ranging from 2.72 to 460 μm. The PSDs obtained were checked to be free of artifacts in the small size classes (~2 μm), as observed by Reynolds et al. (2010) who identified a stray light problem in this range. This stray light contamination problem was almost negligible in our samples, notably because of the red wavelength (670 nm) of the LISST sensor used in our study, while Reynolds et al. (2010) LISST sensor measured at 532 nm.

The following power law function was fitted to the PSD data:

$$N(D) = No*(D/Do)^{-j} \quad (3)$$

where $N(D)$ is the particle number density($\sim/m^3\,\mu m^{-1}$), No is $N(D)$ at Do, Do is a reference diameter (μm), D is the diameter in the center of the size class (μm) and j is the slope of the PSD (also known as Junge exponent). The following sizes ranges were considered to estimate j: 4.5 to 280 μm, 4.5 to 104 μm and 4.5 to 10 μm. The size bins lower than 4.5 μm and higher than 280 μm were avoided in the calculation as the conversion of LISST measurements is known to overestimate particle volumes for these sizes (Y. Agrawal, personal communication).

In the case of non-absorbing particles following a Junge size distribution, $b_p = c_p$ and the c_p spectral slope, γ_{cp}, is simply related to the slope (j) of the particle size distribution (PSD) according to Morel (1973):

$$j = \gamma_{cp} + 3 \quad (4)$$

Boss et al. (2001a) reported another equation which extends this to the case of mineral absorbing particles:

$$j = \gamma_{cp} + 3 - 0.5\exp(-6\gamma_{cp}) \quad (5)$$

3. Results and discussion

3.1. Spatial and seasonal variations of biogeochemical parameters

Fig. 3 shows the seasonal, spatial and inter-annual (2005–2009) variability of CHL, TSM and TSM organic content (OSM, in %) in the three zones identified in the Southern North Sea (Fig. 2). The 2005–2008 dataset highlights significant seasonal variations in CHL and OSM/TSM in the SCZ and MSNS with maximum values in April. The spatial variability of TSM is more important than the seasonal one, with higher concentrations in the SCZ and TCZ and lower concentrations in the MSNS. Spatial variability in CHL is also significant with large differences between the TCZ, the MSNS and the SCZ where concentrations up to 71 mg m^{-3} were recorded. The fraction of organic TSM (OSM/TSM) is maximal in the MSNS and minimal in the TCZ. Inter-annually, maximum CHL concentrations are found in April 2008 in the TCZ and MSNS and

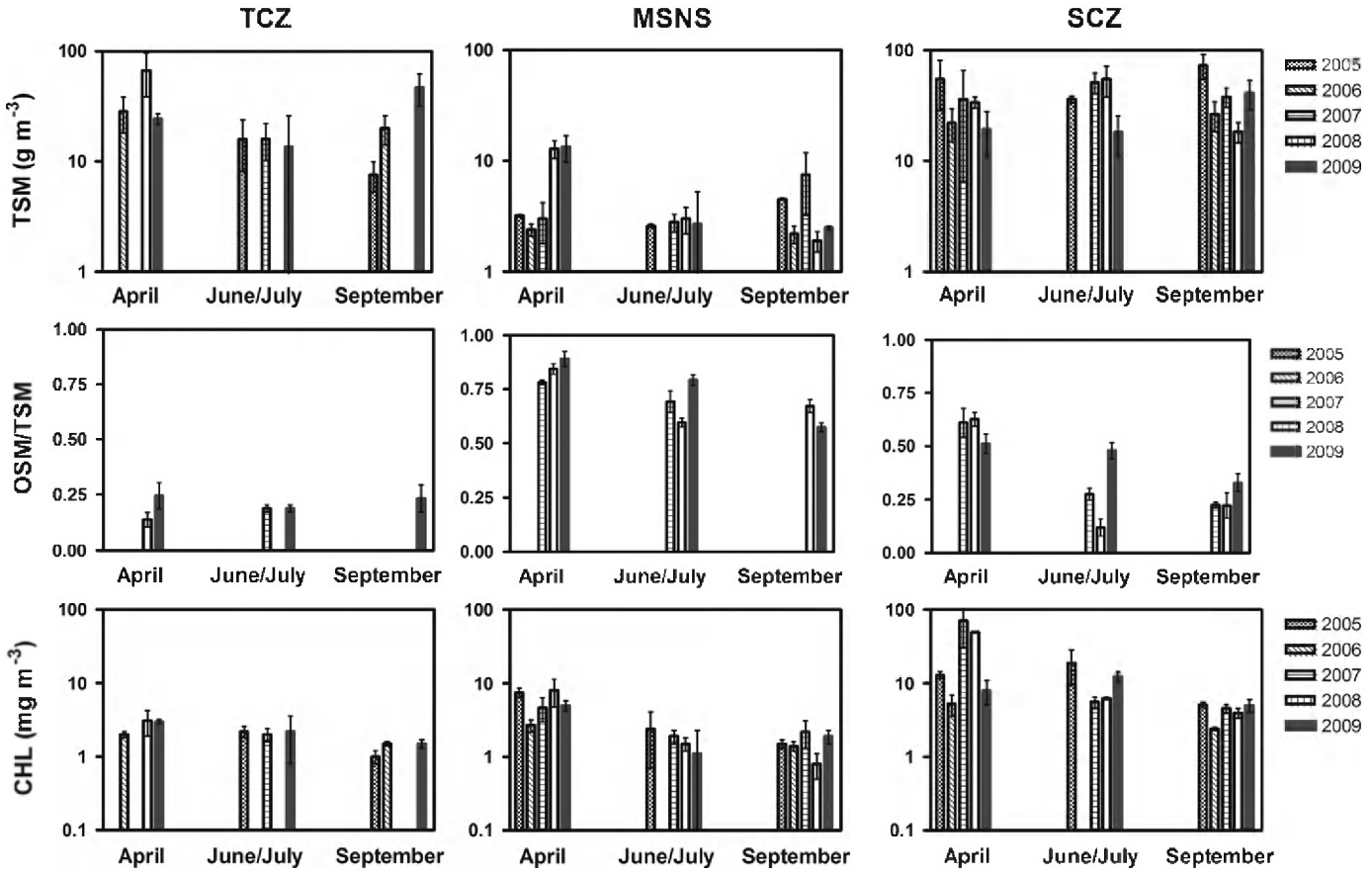

Fig. 3. Inter-annual variability (2005–2009) of key biogeochemical parameters for the three geographical zones (TCZ left panel, MSNS central panel, SCZ right panel) and for the three cruises (mean ± standard deviation). Note the logarithmic scale for TSM and CHL. First row: TSM concentrations (g m^{-3}); second row: fraction of organic TSM, OSM/TSM; third row: CHL concentrations (mg m^{-3}). 2009 measurements have been highlighted in dark gray bars.

in 2007 in the SCZ revealing the occurrence of intense spring phytoplankton blooms those years. In comparison, the 2009 data are consistent with the variations of these parameters in the three areas, except for the low April CHL concentrations recorded in the SCZ as compared to maximum April 2007 and 2008 CHL concentrations.

The detailed analysis of the 2009 spatial and seasonal variability of these biogeochemical parameters is illustrated in Fig. 4. The measured surface CHL and TSM concentrations exhibited variations along the SCZ–TCZ transect. The highest and lowest CHL concentrations were respectively observed in the SCZ and TCZ; similarly, TSM concentration was the highest nearshore and the lowest in the MSNS (Fig. 4 left panel, Table 1). For the three cruises, CHL reached maxima in the SCZ (maximum of 15.8 mg m^{-3} sampled in April during the spring bloom) comparatively to the TCZ (4.2 mg m^{-3} in June). The lowest CHL concentration (0.3 mg m^{-3}) was measured in the MSNS in June. The highest TSM concentrations were measured in the TCZ and SCZ in September (87.3 g m^{-3} and 64 g m^{-3}, respectively) resulting from strong wind effects enhancing resuspension of bottom sediments in these shallow waters. The maximum TSM values recorded in the SCZ in April and September were observed slightly away from the coast (stations 2 and 3, respectively) suggesting that resuspension processes were more important than direct TSM inputs from the Scheldt river. The lowest TSM concentration was measured in the MSNS in June (1.2 g m^{-3}). The fraction of organic TSM (OSM/TSM) was systematically lower in the TCZ (minimum of 0.11 in September) but significant in the SCZ (> 0.17) and the MSNS where it reached 0.48 in April (Fig. 4 left panel).

The above results show that the three zones identified in the Southern North Sea have specific characteristics in terms of

Table 1
Variability of biogeochemical parameters (CHL in mg m^{-3}, TSM in g m^{-3}, OSM/TSM ratio) for all field 2009 data and for each area identified in the Southern North Sea. Mean values and standard deviations (S.D.) are shown.

Cruise	Area	CHL		TSM		OSM/TSM	
		Mean	S.D	Mean	S.D	Mean	S.D
April	All	5.3	3.8	19.0	11.1	0.36	0.09
	TCZ	3.0	0.3	24.4	5.4	0.27	0.03
	MSNS	5.0	1.5	13.3	7.1	0.43	0.05
	SCZ	8.0	5.7	19.4	17.0	0.36	0.08
June	All	5.3	5.6	11.5	10.3	0.25	0.08
	TCZ	2.2	1.4	13.5	12.6	0.19	0.02
	MSNS	1.1	1.2	2.7	2.6	0.33	0.07
	SCZ	12.6	1.9	18.2	7.3	0.23	0.04
Sept	All	2.9	2.1	30.5	28.1	0.22	0.11
	TCZ	1.5	0.4	47.0	30.1	0.16	0.06
	MSNS	1.9	0.7	2.5	0.2	0.33	0.15
	SCZ	5.4	1.9	42.0	20.1	0.18	0.01

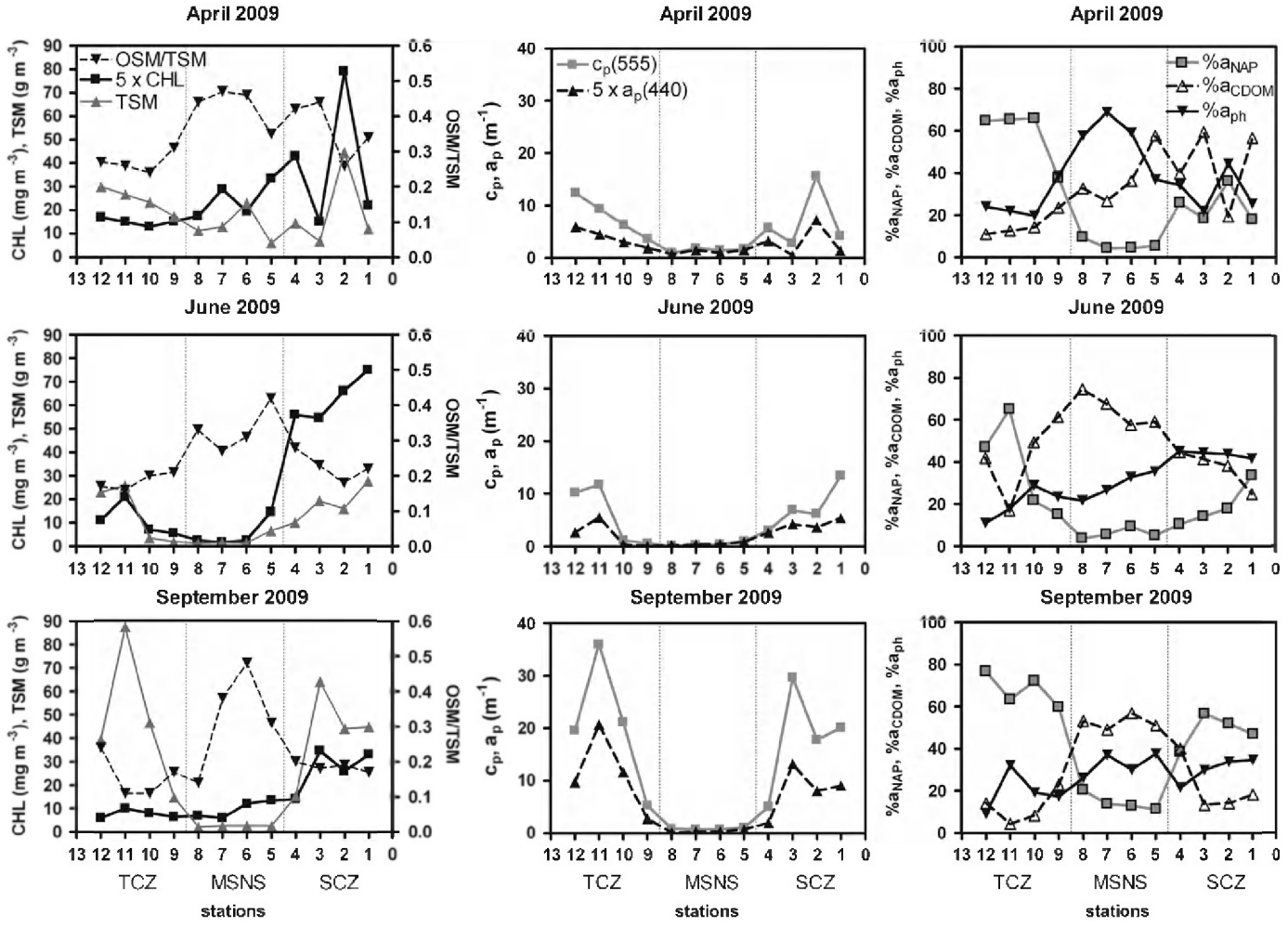

Fig. 4. Variability of biogeochemical parameters (CHL concentrations, mg m^{-3}; TSM. concentrations, g m^{-3}; OSM/TSM ratio), left panel; inherent optical properties: $c_p(555)$ and $a_p(440)$, central panel and respective contributions of non-algal particles ($\%a_{NAP}$), CDOM ($\%a_{CDOM}$) and phytoplankton ($\%a_{ph}$) absorption to total light absorption at 440 nm, right panel; along the SCZ–TCZ transect for the three cruises in 2009.

biogeochemical parameters: high TSM and CHL concentrations close to the coasts and low concentrations in the MSNS. In addition, the composition of particles is specific, being predominantly inorganic in the TCZ, organic in the MSNS and a mixture of both in the SCZ.

Interestingly, differences were found between the SCZ and TCZ. For example, in April the phytoplankton bloom reached higher CHL concentrations in the SCZ than in the TCZ, while the opposite was observed for inorganic TSM. These results can be explained by a different spreading of nutrient- and TSM-rich river plumes in the SCZ and TCZ as shown by the salinity distribution along the transect (Fig. 2) and by resuspension processes. In the SCZ, light penetration and nutrients are sufficient to allow phytoplankton to bloom every spring and summer (Lancelot et al., 1987; Rousseau et al., 2006). Biomass accumulation (mainly *P. globosa* colonies) in the SCZ adds to inorganic particles, thus increasing both CHL and TSM concentrations. In the TCZ, the Thames river discharge did not have a significant influence as suggested by the salinity values (33.8–34.7; Fig. 2), therefore resuspension processes are believed to produce permanent high TSM concentrations that limit light penetration, thus preventing phytoplankton to develop and thus explaining the low CHL concentrations.

The MSNS shows biogeochemical properties more similar to clear open ocean waters with low CHL and TSM concentrations of predominantly organic particles (Bricaud et al., 1998) (Fig. 4 left panel, Table 1). The salinity in this area is ~34.8 indicating the intrusion of Atlantic clear water masses through the Channel (Ruddick and Lacroix, 2006).

The observed spatial variation in the biogeochemical parameters was already observed in the North Sea by Babin et al. (2003a, 2003b) who reported TSM and CHL concentrations varying by two orders of magnitude from offshore to nearshore waters. Spatial variations of CHL along the SCZ–TCZ transect were previously documented using MERIS yearly median satellite images in 2003 (Peters et al., 2005) with higher CHL concentrations (~30 mg m^{-3}) in the SCZ than the TCZ (7–10 mg m^{-3}) and lower concentrations in the MSNS (4–7 mg m^{-3}), which again agrees with our field observations. Seasonal variations were also observed using MERIS monthly median CHL images in 2003, for example in the SCZ, in April, June and September CHL concentrations reached up to 80, 10 and 20 mg m^{-3}, respectively (Peters et al., 2005).

3.2. Variations of the inherent optical properties as a function of particle concentration

The variability of particle attenuation (c_p) and absorption (a_p) coefficients along the SCZ–TCZ transect showed the same trend as that observed for TSM concentrations (Fig. 4 central panel): maximum values along the coasts and minimum values in the MSNS. In this area, minimum $c_p(555)$ was found in June (0.12 m^{-1}) and minimum $a_p(440)$ in September (0.03 m^{-1}). Maximum $c_p(555)$ and $a_p(440)$ of respectively 36.0 and 4.1 m^{-1} were recorded in the TCZ for respectively 29.7 and 2.6 m^{-1} in the SCZ, in September. Reversely, the $c_p(555)$ and $a_p(440)$ recorded in April and June were higher in the SCZ (15.6 and 1.5 m^{-1} and 13.4 and 1.1 m^{-1}, respectively) than in the TCZ (12.4 and 1.5 m^{-1} and 11.7 and 1.1 m^{-1}, respectively). As reported earlier for TSM, in September the maximum IOPs values were measured at stations slightly away from the coast indicating that resuspension processes contribute more to TSM than direct inputs from rivers (Fig. 2).

The particle attenuation coefficient (c_p) at 555 nm was directly related to total TSM, ISM and OSM concentrations. Table 2 shows the results of linear regressions obtained between TSM, ISM, OSM and c_p. When considering successively the two datasets: the TCZ–SCZ transect in 2009 and the Belgian–Dutch–English marine areas in the 2005–2008 dataset, a robust relationship still stands between TSM and particle attenuation ($R^2 > 0.93$) indicating that $c_p(555)$ is a good proxy for TSM in the whole Southern North Sea. The influence of particle composition on the $c_p(555)$ vs TSM relationship clearly appears when comparing this relationship with the $c_p(555)$ vs ISM and $c_p(555)$ vs OSM relationships, where the slopes of the $c_p(555)$ vs ISM relationships show a better fit (R^2) than those of the $c_p(555)$ vs OSM relationships indicating that inorganic particles control the $c_p(555)$ vs TSM relationship. This is expected as inorganic particles are much more efficient than phytoplankton in terms of light scattering. Another evidence can be seen in the very similar slopes for TCZ and SCZ with high % of inorganic particles ($F=0.200$, $p=0.6594$) which are significantly different from that of the MSNS (with a high OSM/TSM) ($F=33.91$, $p<0.0001$).

We then looked at the respective contributions of phytoplankton, NAP and CDOM absorption to light absorption at 440 nm. Results (Fig. 4 right panel) show that the relative contribution of NAP is a good indicator to distinguish the coastal from the offshore regions of the Southern North Sea. In the MSNS, the NAP contribution was in average lower than 14% while in the SCZ and TCZ it was higher than 14%. Results also show that the phytoplankton contribution to total absorption can be used to distinguish between the two coastal zones. The average phytoplankton contribution was 35% in the SCZ and 22% in the TCZ. In April and June, the CDOM contribution ranged from 10 to 75% for all stations. In the most nearshore and turbid TCZ stations, the contribution of CDOM to light absorption was systematically low (maximum of 17% with exceptions in June).

These results point out that phytoplankton, CDOM and NAP all contributed to the variability of total absorption, although different components dominated in different regions and times of the

Table 2
Linear regression of c_p at 555 nm (m^{-1}) as a function of TSM, ISM and OSM (g m^{-3}) for the Southern North Sea. Slopes, 95% confidence intervals (CI) of the slope and standard deviation of residuals (SDR) are shown. All results are significant at $p<0.0001$ level.

		TSM vs $c_p(555)$					ISM vs $c_p(555)$					OSM vs $c_p(555)$				
		Slope (m^2 g^{-1})	95% CI	SDR	R^2	n	Slope (m^2 g^{-1})	95% CI	SDR	R^2	n	Slope (m^2 g^{-1})	95% CI	SDR	R^2	n
2009	April	0.31	0.24–0.38	2.41	0.89	12	0.45	0.37–0.53	1.93	0.93	12	0.90	0.54–1.25	3.78	0.74	12
2009	June	0.43	0.39–0.47	1.02	0.98	12	0.54	0.49–0.58	0.84	0.99	12	2.03	1.57–2.49	2.24	0.89	12
2009	Sept	0.44	0.41–0.46	1.37	0.99	12	0.51	0.48–0.55	1.95	0.99	12	2.72	2.27–3.17	4.45	0.94	12
2009	TCZ	0.42	0.38–0.45	2.03	0.98	12	0.49	0.45–0.54	2.02	0.98	12	2.28	1.58–2.99	6.60	0.82	12
2009	MSNS	0.10	0.06–0.14	0.60	0.70	12	0.19	0.11–0.26	0.55	0.74	12	0.21	0.11–0.31	0.65	0.64	12
2009	SCZ	0.42	0.39–0.46	1.62	0.99	12	0.53	0.50–0.56	1.28	0.99	12	1.93	1.51–2.36	4.44	0.90	12
2009	All data	0.41	0.38–0.44	2.21	0.97	36	0.50	0.48–0.53	1.71	0.98	36	1.78	1.41–2.14	6.08	0.74	36
2005–2008	All data	0.41	0.40–0.43	3.15	0.93	181	0.52	0.48–0.55	3.69	0.92	93	1.05	0.88–1.22	7.86	0.63	93
2005–2009	All data	0.41	0.40–0.43	3.01	0.93	217	0.51	0.49–0.54	3.25	0.93	129	1.14	0.98–1.29	7.66	0.63	129

year. The variability of light absorption is essentially driven by NAP in the TCZ, by phytoplankton and CDOM in the MSNS and by the three components in the SCZ. These results are slightly different from those obtained by Babin et al. (2003b) in the North Sea reporting a higher average contribution of CDOM to light absorption and equal contributions by NAP and phytoplankton, probably because our study covers different water masses.

3.3. Spectral variations of the specific inherent optical properties as a function of particle composition

In this section, we analyze the spectral variations of those bio-optical parameters that provide information on particle composition and then we study their spatial and seasonal variability at one wavelength.

CHL-specific phytoplankton absorption coefficient. The shape of the a^*_{ph} spectrum differed between seasons and from one optical zone to another. Three peaks were clearly identified in the blue region (412, 436 and 465–467 nm) in the MSNS at all seasons. These absorption peaks are much less marked in both the TCZ and SCZ (Fig. 5), probably due to the presence of CHL degradation products (Hoepffner and Sathyendranath, 1991).

The typical shape of $a^*_{ph}(\lambda)$ measured in April in the MSNS and June in the SCZ, notably with an absorption peak at 467 nm, indicates the presence of *P. globosa* (Astoreca et al., 2009a). The shape obtained in June in the MSNS is different from that of *P. globosa* in that the peaks at 412 and 465–467 nm show a different ratio (0.84) from that corresponding to *P. globosa* (0.92), suggesting a different phytoplankton composition in this area. It could also indicate a dominance of smaller phytoplankton cells compared to April, as suggested by the higher $a^*_{ph}(440)$ found for this area. As shown by Bricaud et al. (2004), $a^*_{ph}(440)$ is partly modulated by the size of phytoplankton cells, with higher $a^*_{ph}(440)$ for small cells and lower $a^*_{ph}(440)$ for large cells. The higher $a^*_{ph}(440)$ values found in June in the MSNS correspond to a smaller average cell size compared to April as confirmed by phytoplankton microscopy counts (not shown). Surprisingly, $a^*_{ph}(440)$ values as high as the one found for September in the TCZ are most probably related to high concentrations of degradation pigments.

Our results highlight significant differences of $a^*_{ph}(440)$ between the three optical zones (Fig. 5, Table 3). In April and September, $a^*_{ph}(440)$ was higher in the TCZ than in the MSNS and SCZ; no difference was found for $a^*_{ph}(440)$ between MSNS and SCZ. In June, $a^*_{ph}(440)$ in the MSNS was higher compared to SCZ but shows no difference with TCZ.

Mass-specific NAP absorption coefficient. For all cruises, the shape of the mass-specific NAP absorption coefficient spectra, $a^*_{NAP}(\lambda)$, exhibited an exponential increase towards the UV. Interestingly, slight changes in the spectral slope are observed in the TCZ at 450 and at 575 nm becoming steeper towards the UV (Fig. 5). Such changes in the spectral shape of $a^*_{NAP}(\lambda)$ spectra have been already observed by Babin et al. (2003b) and ascribed to iron oxides associated to mineral particles. This could be the case in the TCZ where the proportion of inorganic particles is much higher than in the two other optical zones identified in the Southern North Sea (Fig. 4).

The $a^*_{NAP}(440)$ values also showed differences between the three zones identified, with maximum values in the TCZ and

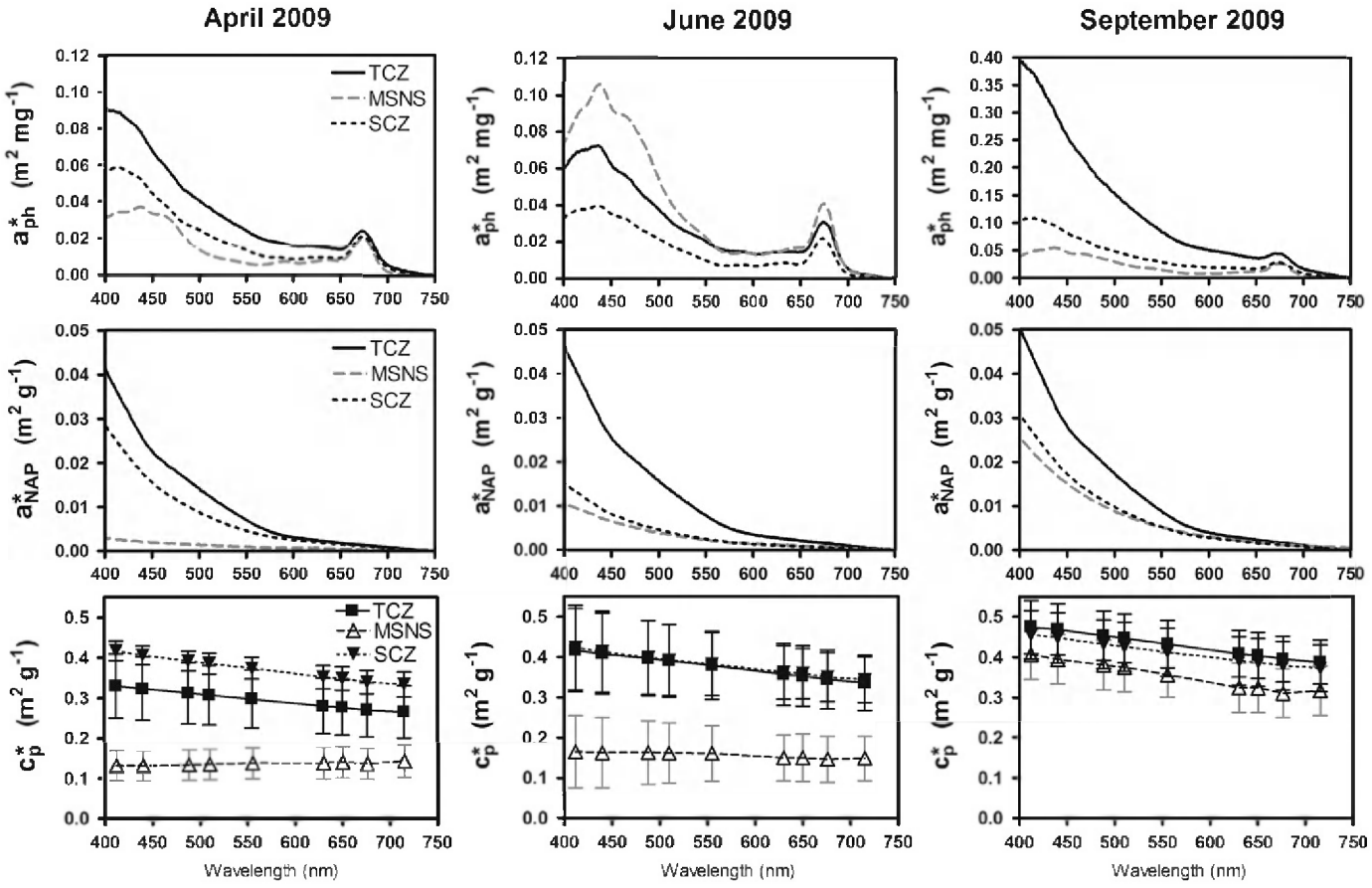

Fig. 5. Seasonal variations of mass-specific IOPs: phytoplankton absorption (a^*_{ph} in $m^2\ mg^{-1}$, first row), non-algal particle absorption (a^*_{NAP} in $m^2\ g^{-1}$, second row) and particle attenuation (c^*_p in $m^2\ g^{-1}$, third row). Each spectrum corresponds to an average of each of the three geographical zones in 2009. Note the different scale in the first row. Standard deviations are added for c^*_p spectra.

Table 3
Variability of mass-specific optical coefficients a^*_{ph} ($m^2\ mg^{-1}$), a^*_{NAP} ($m^2\ g^{-1}$) and c^*_p ($m^2\ g^{-1}$) for all field 2009 data and for each area identified in the Southern North Sea. Mean values and standard deviations (S.D) are shown.

Cruise	Area	a^*_{ph} (440)		a^*_{NAP} (440)		c^*_p (555)	
		Mean	S.D	Mean	S.D	Mean	S.D
April	All	0.051	0.017	0.013	0.010	0.270	0.127
	TCZ	0.077	0.016	0.026	0.002	0.298	0.102
	MSNS	0.037	0.008	0.002	0.002	0.138	0.094
	SCZ	0.052	0.007	0.018	0.005	0.374	0.027
June	All	0.073	0.045	0.015	0.012	0.308	0.129
	TCZ	0.071	0.015	0.029	0.006	0.379	0.084
	MSNS	0.105	0.059	0.007	0.004	0.161	0.068
	SCZ	0.039	0.016	0.009	0.006	0.382	0.078
September	All	0.100	0.069	0.024	0.008	0.396	0.065
	TCZ	0.291	0.265	0.032	0.005	0.432	0.059
	MSNS	0.054	0.016	0.017	0.006	0.356	0.061
	SCZ	0.092	0.034	0.020	0.004	0.412	0.060

minimum values in the MSNS whatever the seasons (Fig. 5, Table 3); but no clear seasonal variation of a^*_{NAP} could be observed in the TCZ. The highest value was recorded in September in the TCZ ($0.032 \pm 0.005\ m^2\ g^{-1}$) and the lowest in April in the MSNS ($0.002 \pm 0.002\ m^2\ g^{-1}$).

The average $a^*_{NAP}(440)$ measured in April and September in the TCZ and SCZ ($0.023 \pm 0.007\ m^2\ g^{-1}$) is close to the average $a^*_{NAP}(443)$ value reported by Babin et al. (2003b) in the North Sea dominated by inorganic particles ($0.033 \pm 0.016\ m^2\ g^{-1}$) and by Bowers and Bindings (2006) for inorganic particles in the Irish Sea ($0.0235\ m^2\ g^{-1}$). This confirms the predominance of inorganic particles in these zones. As shown by the relationship found between $a^*_{NAP}(440)$ and the ISM/TSM ratio, $a^*_{NAP}(440)$ direct increases when the percentage of inorganic particles increases (Fig. 6A). The minimum $a^*_{NAP}(440)$ values are also comparable to those found by Blondeau-Patissier et al. (2009) in non-estuarine waters of the Great Barrier Reef (range: 0.001–0.02 $m^2\ g^{-1}$) for clear waters as in the MSNS.

TSM-specific particle attenuation. The spectral shape of $c^*_p(\lambda)$ in the TCZ and SCZ typically decreased towards the NIR (negative slopes) (Fig. 5). The spectral shape of $c^*_p(\lambda)$ in the MSNS showed minima at 440 nm and increased towards the NIR (positive slope) in April while it was flat in June.

For all cruises maximum $c^*_p(555)$ values were observed in the TCZ and SCZ while minimum values were observed in the MSNS (Fig. 5, Table 3). Note that the difference between the maximum and minimum $c^*_p(555)$ found in September is much lower than the differences found in April and June, suggesting a more homogenous particle composition in September in the Southern North Sea. This can also be seen in the a^*_{NAP} data in September where the three spectra are closer to each other than in the other seasons.

A linear relationship was found between $c^*_p(555)$ and the ISM/TSM ratio for all 2009 data (Fig. 6B). Although the low R^2 (0.39), a marked trend can be clearly seen especially for ISM/TSM ratio >0.70 suggesting once again that inorganic particles are driving the variability of $c^*_p(555)$ in the Southern North Sea.

Seasonally, differences were found in the TCZ between April and June, and lower $c^*_p(555)$ values were recorded in the MSNS in April and June but not in September, possibly resulting from variations of particle composition. The MSNS was dominated by organic particles in April ($>40\%$) but not in September which is supported by the corresponding c^*_p values. On average in 2009 $c^*_p(555)$ was equal to $0.33 \pm 0.12\ m^2\ g^{-1}$ in the sampled Southern North Sea waters which is close to the $b^*_p(555)$values reported by Doxaran et al. (2009) in the same region ($0.35 \pm 0.08\ m^2\ g^{-1}$). Babin et al. (2003a) did measure significantly higher values ($0.54\ m^2\ g^{-1}$ on average in subregions of the North Sea) as the OSM/TSM they sampled was particularly low (0.17). This clearly highlights the strong regional variations of the suspended matter composition in the Southern North Sea and the impact on their mass-specific optical properties.

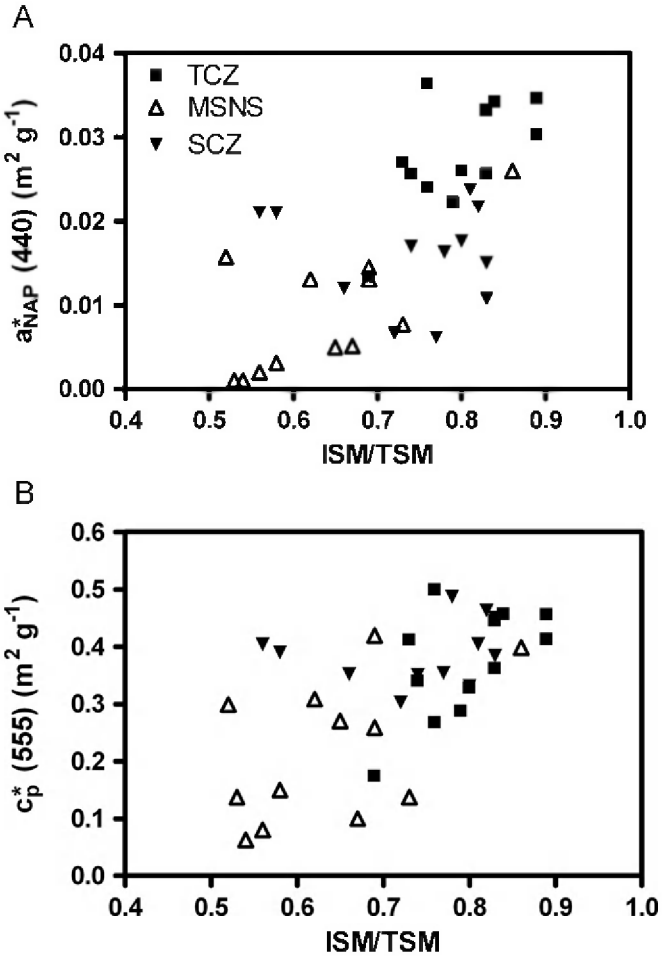

Fig. 6. Scatter plots of the mass-specific: non-algal particle absorption at 440 nm (a^*_{NAP}, in $m^2\ g^{-1}$) as a function of the ratio ISM/TSM (A) and particle attenuation (c^*_p in $m^2\ g^{-1}$) at 555 nm as a function of the ratio ISM/TSM (B) for the SCZ, MSNS and TCZ in 2009.

One of the most striking results of this study concerns the spectral variations of the c_p coefficient. When considering γ_{cp}, a high range of variation is observed from -0.3 to 0.7 on the 2009 data (Fig. 7A). Note that negative γ_{cp} values were also found when considering the 440–715 nm spectral range. Negative γ_{cp} values were identified during the April cruise in the MSNS and values close to 0 were observed in June at offshore stations where the spectral shape of c_p did no longer follow a power law ($R^2 < 0.50$ for the fit of Eq. (2) to the c_p data). These are stations where the particulate absorption significantly affects the spectral shapes of b_p and c_p resulting in troughs at the maximum absorption wavelengths (440 and 676 nm). Babin et al. (2003a) and Doxaran et al. (2009) already observed and explained these features to be related to pigment absorption by algae for North Sea data. Negative γ_{bp} slopes (as low as -1) have been reported by Snyder et al. (2008) in US coastal waters and negative γ_{cp} slopes have been reported by Sullivan et al. (2005) for concentrated phytoplankton layers of Monterey Bay. In our Southern North Sea dataset, negative γ_{cp} slopes were found when the NAP contribution to total absorption was minimum (<0.2). This situation occurred during the phytoplankton spring bloom at offshore stations corresponding to the less turbid waters sampled where both the a_p and c_p signals were clearly dominated by phytoplankton. An empirical relationship was

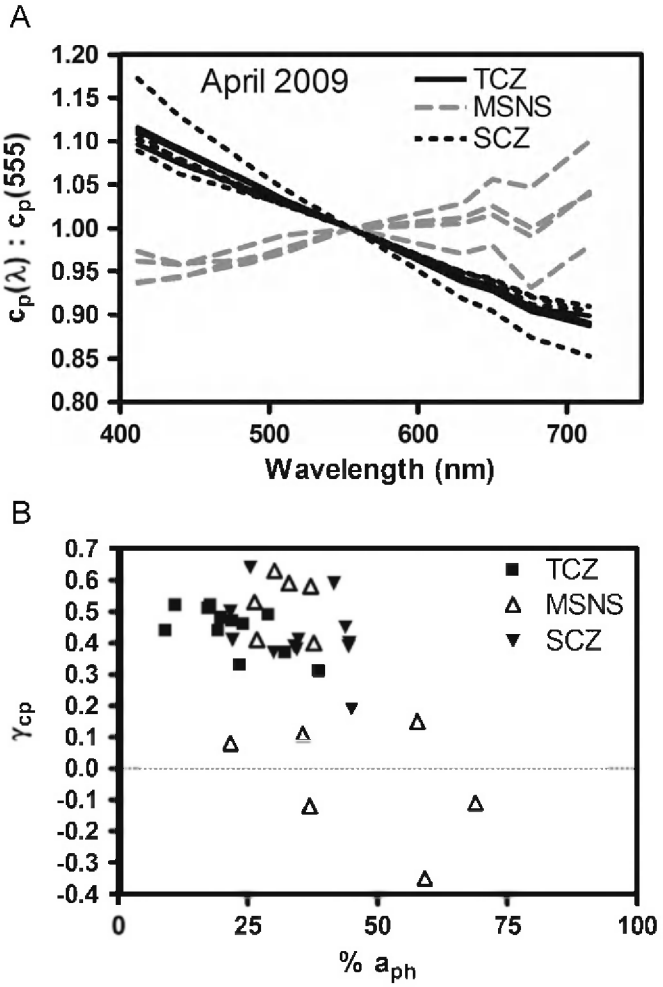

Fig. 7. Spectral variations of c_p, normalized at 555 nm, in April 2009 for the three geographical zones (A). Scatter plot of the c_p spectral slope, γ_{cp}, as a function of the percentage contribution of phytoplankton to total absorption, $\%a_{ph}$ for the SCZ, MSNS and TCZ in 2009 (B).

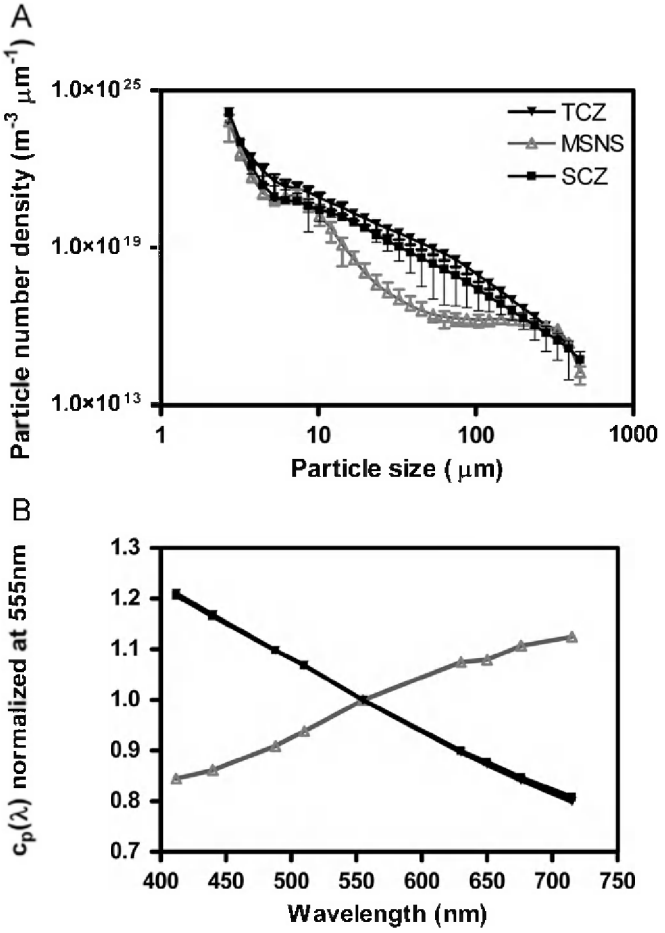

Fig. 8. Average PSDs (with standard deviation bars) measured in the SCZ, MSNS and TCZ in April 2009 (A). Corresponding c_p spectra, normalized at 555 nm, computed using Mie theory when using the measured PSDs as inputs (see the text for details) (B).

found to try to explain the variations of γ_{cp} as a function of particle composition (Fig. 7B). It is a linear relationship between γ_{cp} and the % contribution of phytoplankton to total absorption, $\%a_{ph}$, with negative γ_{cp} found for $\%a_{ph}$ higher than 37%. Note that this parameter alone cannot explain the negative slopes since positive slopes are also found for $\%a_{ph}$ higher than 50%. However, this result highlights the importance of organic particles on the spectral shape of c_p.

The effect of TSM composition on the spectral variations of c_p was also observed in laboratory data (not shown). A mixture of phytoplankton species typical of the Southern North Sea, show a c_p spectrum with troughs corresponding to CHL absorption peaks at 440 and 675 nm. The addition of increasing amounts of TSM to this phytoplankton mixture first only slightly impacted the γ_{cp} spectral slope, then progressively flattened the c_p spectral shapes masking the influence of the CHL absorption peaks. The c_p spectral shape then gradually moved to a flat shape (that can be modeled with a power-law function decreasing from short visible to near-infrared wavelengths) which is typical of sediment-dominated coastal waters (Boss et al., 2001a; Doxaran et al., 2009).

3.4. *Variations of the inherent optical properties as a function of particle size*

The PSDs measured close to the coasts (TCZ and SCZ) and in offshore waters (MSNS) in April clearly differed (Fig. 8A). Coastal PSDs typically show a more power-law shape (Eqs. (4) and (5)) although a peak is seen in the SCZ at 7 μm, while offshore PSDs (MSNS; Fig. 8A) show a bimodal shape with two peaks corresponding to particle diameters of 7 and 280 μm respectively. In June and September, offshore PSDs show a flatter shape resembling that of coastal PSDs in April (not shown). The PSD shape with one or more peaks has been already observed by Reynolds et al. (2010) and associated to the presence of high percentages of organic material in the water where the peaks correspond to distinct plankton populations.

The γ_{cp} spectral slope is related to the PSD slope (j) when particles are non-absorbing, spherical, homogenous and distributed in size according to an unbounded power law (Morel, 1973; Boss et al., 2001a). The variations of the PSD slope (j), calculated for different size ranges and using Eqs. (4) and (5), as a function of γ_{cp} are shown in Fig. 9. It shows that j tends to follow a power law shape (Morel 1973 model) when calculated including bigger particles (4.46–280 mm). When smaller particle size ranges are considered, the relationship between j and γ_{cp} becomes noisy especially for values of γ_{cp} between 0.25 and 0.70. Actually Eqs. (4) and (5) were valid (within $\pm$ 0.05) only for 6 stations out of 36, 4 of them in the coastal zones and 2 of them in the MSNS in September dominated by inorganic particles. It is clear from these results that the power law model is not the best model to describe the PSD in the Southern North Sea, especially during the phytoplankton bloom as particles are highly absorbing in the visible part of the spectrum and non-homogenous because of

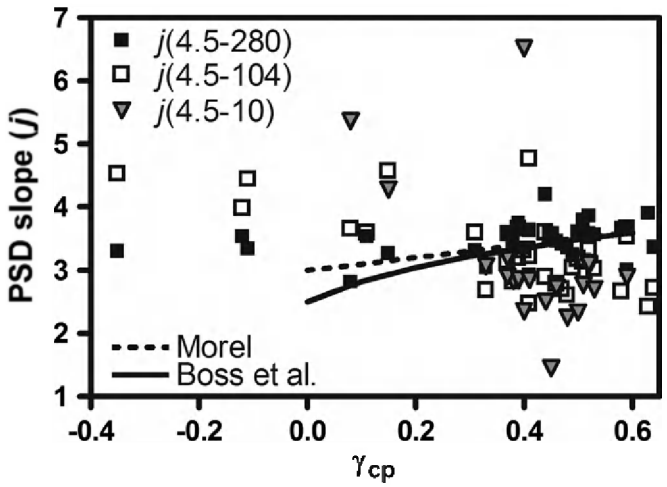

Fig. 9. Variations of the power-law PSD slope (j) as a function of the c_p spectral slope (γ_{cp}) for field data in 2009. The Morel (1973), ($j=\gamma_{cp}+3$) and Boss et al. (2001a, 2001b), ($j=\gamma_{cp}+3-0.5\exp(-6\gamma_{cp})$) models are also shown. Note that j was calculated for different size ranges.

a mixture of *P. globosa* colonies, diatoms and inorganic material. This conclusion agrees with Reynolds et al. (2010) who state that the power law model fails to capture the complexities of the PSD of dynamic populations found in coastal waters. Another cause for the highly scattered relationship between j and γ_{cp} could be that the instrument are not sampling the same particles: either due to different sampling strategies (while the LISST is viewing the particles in situ, for the ac-9 the water is collected, shaken then passed through the ac-9 tubes by gravimetry which could significantly alter the PSD) or due to different acceptance angles of the instruments (see Boss et al., 2009).

The PSDs measured in April in the MSNS had a bimodal shape significantly different from a power-law size distribution. Remarkably, negative γ_{cp} slopes were measured at these stations. In the previous chapter we have seen that γ_{cp} negative slopes were not fully explained by $\%a_{ph}$, so that Mie computations were used to explain the occurrence of such negative slopes. The code already presented by Doxaran et al. (2009) was used to calculate c_p at the 25-cm ac-9 wavelengths: 412, 440, 488, 510, 555, 630, 650, 676 and 715 nm. The typical PSDs measured with the LISST in the SCZ, MSNS and TCZ (Fig. 8A), i.e., the number of equivalent spherical particles at size bins ranging from 4.5 to 280 μm, were used as inputs. A power-law function was also fitted to these distributions. The real part of the particle refractive index was set to 1.05 for the MSNS (predominantly phytoplankton particles) and to 1.15 in the SCZ and TCZ (inorganic particles). Typical spectral values of the imaginary part of the refractive index were taken from Babin et al. (2003a) (see their Fig. 8) for phytoplankton (MSNS) and inorganic particles (SCZ and TCZ). Results show that c_p varies with wavelength as a power-law function in the SCZ and TCZ (Fig. 8B), where the measured PSDs also follow a power-law function as a first approximation. A negative c_p spectral slope ($\gamma_{cp}=-0.31$) is obtained for the MSNS, close to the slope measured with the ac-9 ($\gamma_{cp}=-0.35$). A similar negative slope ($\gamma_{cp}=-0.34$) is obtained if non-absorbing particles are considered in the computations (imaginary refractive index set to 0). The simple conclusion is that the negative c_p slope is due to the bimodal shape of the PSD and not to particulate absorption effects. The typical PSD measured in the MSNS was then modified in order to remove the peaks respectively located around 7 and 280 μm. The best-fitted power-law function was used to calculate the number of particles within the size range covered by each peak, in order to smooth the PSD. If the peak at 280 μm is removed while the one at 7 μm remains, the c_p slope is still negative and does not vary significantly. Now if the peak at 7 μm is removed while the one at 280 μm remains, the c_p slope changes dramatically and becomes positive ($\gamma_{cp}=0.82$). The conclusion is that the negative c_p slope results from the bloom of phytoplankton particles around the size of 7 μm. If the magnitude of this peak increases, the c_p slope is even more negative. Note that this result is only obtained in the case of organic particles. In the case of inorganic particles, a similar peak at 7 μm over a power-law size distribution has a very limited impact on c_p spectral variations. Therefore the occurrence of a negative c_p slope clearly identifies the bloom of phytoplankton particles around the size of 7 μm in offshore waters away from direct inputs of inorganic particles.

Indeed, phytoplankton microscopy counts performed on *P. globosa* cultures reveal a peak of cell number of 5.3 μm diameter (not shown). Rousseau et al. (2007) found that *P. globosa* single cells of 7.9 ± 0.9 μm reduce their diameter to 5.9 ± 0.6 μm after fixation with lugol. This clearly suggests that the peak identified at 7 μm in the PSD of April in the MSNS corresponds to single cells of *P. globosa*.

4. Conclusion and perspectives

Based on field measurements carried out in 2009 in the Southern North Sea, our results show that spatial variability of CHL and TSM concentrations, fraction of organic/inorganic TSM and also IOPs was clearly predominant over seasonal variability. Generally high values were found in the coastal zones and lower values in offshore areas. This characterization allowed the classification of the Southern North Sea into three geographical zones: the SCZ characterized by high concentrations of CHL and TSM and high values of IOPs; the MSNS with very low concentrations of CHL and TSM, low IOPs values but high particulate organic content; and the TCZ with very low particulate organic particle content, low CHL concentrations but high concentration of TSM and IOPs. The global absorption budget is driven by NAP, phytoplankton and CDOM, which all contribute seasonally to the variability of total absorption. The a^*_{ph} coefficient varied considerably both spatially and seasonally and its spectral shape differed from the coasts (SCZ and TCZ) to offshore (MSNS). The a^*_{NAP} coefficient varied spatially with much higher values in the TCZ than in the SCZ and MSNS. The c^*_p coefficients showed higher values in the TCZ and SCZ (where suspended particles are mostly inorganic) than in the MSNS (where suspended particles are predominantly phytoplankton), although in September the three zones showed similar values (as strong tidal currents contributed to mix inorganic and phytoplankton particles). It was found that inorganic particles explain most of the variability of c^*_p in the Southern North Sea, as highlighted using the ISM/TSM ratio. The spectral variations of c_p were also controlled by the composition of TSM. The spectral slope of c_p (γ_{cp}) varied considerably with values ranging from -0.3 to 0.7. Negative γ_{cp} values were reported at offshore stations during the April phytoplankton bloom. On the one hand, the variations in γ_{cp} cannot be explained by the percentage contribution of phytoplankton to total absorption alone. On the other hand, the PSDs found in the Southern North Sea greatly varied with flat power-law shapes found in coastal zones to a bimodal shape found in offshore zones dominated by *P. globosa*. Using Mie computations it was found that the negative c_p slope is due to the bloom of phytoplankton around the size of 7 μm, which corresponds to single cells of *P. globosa*. The theoretical relation between the PSD slope (j) and γ_{cp} did not work in the offshore Southern North Sea during the bloom. Other models to describe the PSD shape may need to be tested, e.g. Gaussian, log-normal or two-component distributions (Jonasz, 1983, 1987; Risovic, 1993). The actual relationship between γ_{cp} and j in coastal waters characterized by mixtures of inorganic particles and phytoplankton still requires further investigation.

However, our results already have a direct application when considering field optical measurements carried out by autonomous platforms such as bio-optical profiling floats (Boss et al., 2008; Claustre et al., 2009) or gliders which complement satellite observations by providing information within the water column. With the installation of a spectral attenuation meter in these packages in the Southern North Sea it will be possible now to detect negative γ_{cp} slopes and to identify the presence of *P. globosa* at least in the MSNS region.

Based on these results, the Southern North Sea proves to be representative of complex coastal waters characterized by strong spatio-temporal variations of its bio-optical constituents, where the development of robust regional ocean color algorithms is challenging. The inversion of bio-optical parameters, such as the CHL and TSM concentrations, from remote sensing reflectance relies on further information and/or knowledge of the specific IOPs and their variability. Specific IOPs variability that is not accounted for in the retrieval algorithms will directly impact on the uncertainty of the retrieved products. A potential approach to be applied in coastal waters where the variability of the remote sensing reflectance is driven by several optically active water components is the one proposed by Lubac and Loisel (2007). They suggest that classification of pixels according to class-specific IOPs algorithms to retrieve the concentrations of biogeochemical parameters should be applied before inversion of bio-optical parameters in these complex environments. Indeed they found that their remote sensing reflectance dataset could be classified into 5 different classes each one having its own set of water constituents' characteristics. In this direction, we suggest that the development of regional or class-specific IOPs algorithms represents an interesting alternative to retrieve bio-optical parameters from remote sensing in such complex environments. The classification of the Southern North Sea into three different optical zones, as proposed in this study, could significantly improve the algorithms for IOPs retrieval from remote sensing reflectance in the area.

In the Southern North Sea various CHL and TSM remote sensing algorithms have been developed (Ruddick et al., 2001; Gons et al., 2002; Eleveld et al., 2008; Nechad et al., 2010). For example, most of the TSM retrieval algorithms rely on several IOPs assumptions, generally the mass-specific IOPs are taken as constant. Doerffer (2006) suggests that the MERIS standard products be considered as IOP products which could be recalibrated on a regional basis if there is sufficient knowledge of mass-specific IOPs, such as b_p^* (or c_p^*) or a_{ph}^*, to provide CHL and TSM as final products. In the Southern North Sea a high variability was found in the mass-specific IOPs since the particle composition and size distribution were observed to vary significantly spatially and seasonally from inorganic (close to the coasts) to organic (in the MSNS during the spring phytoplankton bloom). This implies that retrieval algorithms could be different from one area to another as their mass-specific IOPs will vary with different types of particles. Seasonally, the TCZ and the MSNS showed the least variability in terms of particle type, being respectively dominated by inorganic and organic particles. This gives an indication that a single retrieval algorithm can be used whatever the season in these areas. For the SCZ this could not be possible since the seasonal variability in IOPs is mostly driven by the spring phytoplankton bloom.

Acknowledgments

This study was funded by the STEREO program of the Belgian Federal Science Policy Office in the framework of the BELCOLOUR (SR/00/003), BELCOLOUR-2 (SR/00/104) and BELSIOP (SR/11/83) projects and by the PRODEX program in the framework of the BELMER (C90224) project. The captains and crew of the R.V. Belgica are thanked for their assistance with seaborne measurements. J.-Y. Parent is acknowledged for help with field measurements. MUMM and VLIZ are thanked for loan of their LISSTs. G. Dall'Olmo and D.G. Bowers are acknowledged for constructive comments that helped improve the manuscript.

References

Astoreca, R., Ruddick, K., Van Mol, B., Rousseau, V., Parent, J.-Y., Lancelot, C., 2006. Variability of the inherent and apparent optical properties in a highly turbid coastal area: Impact for the calibration of Remote Sensing algorithms. EARsEL eProceedings 5, 1–17.

Astoreca, R., Rousseau, V., Ruddick, K., Knechciak, C., Van Mol, B., Parent, J.-Y., Lancelot, C., 2009a. Development and application of an algorithm for detecting *Phaeocystis globosa* blooms in the Case 2 Southern North Sea waters. Journal of Plankton Research 31, 287–300.

Astoreca, R., Rousseau, V., Lancelot, C., 2009b. Coloured dissolved organic matter (CDOM) in Southern North Sea waters: optical characterization and possible origin. Estuarine, Coastal and Shelf Science 85, 633–640.

Babin, M., Morel, A., Fournier-Sicre, V., Fell, F., Stramski, D., 2003a. Light scattering properties of marine particles in coastal and open ocean waters as related to the particle mass concentration. Limnology and Oceanography 48, 843–859.

Babin, M., Stramski, D., Ferrari, G.M., Claustre, H., Bricaud, A., Obolensky, G., Hoepffner, N., 2003b. Variations in the light absorption coefficients of phytoplankton, nonalgal particles, and dissolved organic matter in coastal waters around Europe. Journal of Geophysical Research 108, 3211–3231.

Blondeau-Patissier, D., Brando, V., Oubelkheir, K., Dekker, A., Clementson, L., Daniel, P., 2009. Bio-optical variability of the absorption and scattering properties of the Queensland inshore and reef waters, Australia. Journal of Geophysical Research 114, C05003. doi:10.1029/2008JC005039.

Boss, E., Twardowski, M.S., Herring, S., 2001a. Shape of the particulate beam attenuation spectrum and its inversion to obtain the shape of the particulate size distribution. Applied Optics 40, 4885–4893.

Boss, E., Twardowski, M.S., Herring, S., 2001b. Shape of the particulate beam attenuation psectrum and its inversion to obtain the shape of the particulate size distribution. Applied Optics 40, 4885–4893.

Boss, E., Swift, D., Taylor, L., Brickley, P., Zaneveld, R., Riser, S., Perry, M.J., Strutton, P.G., 2008. Observations of pigment and particle distributions in the western North Atlantic from an autonomous float and ocean color satellite. Limnology and Oceanography 53, 2112–2122.

Boss, E., Slade, W., Behrenfeld, M., Dall'Olmo, G., 2009. Acceptance angle effects on thebeam attenuation in the ocean. Optics Express 17, 1535–1550.

Bowers, D.G., Bindings, C.E., 2006. The optical properties of mineral suspended particles: A review and synthesis. Estuarine, Coastal and Shelf Science 67, 219–230.

Bricaud, A., Morel, A., Babin, M., Allali, K., Claustre, H., 1998. Variations of light absorption by suspended particles with chlorophyll a concentration in oceanic (case 1) waters: Analysis and implications for bio-optical models. Journal of Geophysical Research 103 (31), 033-31.044.

Bricaud, A., Claustre, H., Ras, J., Oubelkheir, K., 2004. Natural variability of phytoplankton absorption in oceanic waters: Influence of the size structure of algal populations. Journal of Geophysical Research, 109. doi:10.1029/2004JC002419.

Chester, R., 2000. Marine Geochemistry. Blackwell Science, U.K.

Claustre, H., Bishop, J., Boss, E., Bernard, S., Berthon, J.-F., Coatanoan, C., Johnson, K., Lotiker, A., Ulloa, O., Perry, M.J., D'Ortenzio, F., Fanton D'Andon, O., Uitz, J., 2009. Bio-optical profiling floats as new observational tools for biogeochemical and ecosystem studies: Potential synergies with ocean color remote sensing, in Proceedings of the "OceanObs'09: Sustained Ocean Observations and Information for Society" Conference (Vol. 2), Venice, Italy, pp. 21–25.

Doerffer, R., 2006. How to determine IOPs from MERIS data, in Danesy D. (Ed.). MAVT-2006, Proceedings of the Second Working Meeting on MERIS and AATSR Calibration and Geophysical Validation, Frascati, Italy, pp. 1–3.

Doxaran, D., Babin, M., Leymarie, E., 2007. Near-infrared light scattering by particles in coastal waters. Optics Express 15, 12834–12849.

Doxaran, D., Ruddick, K., McKee, D., Gentili, B., Tailliez, D., Chami, M., Babin, M., 2009. Spectral variations of light scattering by marine particles in coastal waters, from visible to near infrared. Limnology and Oceanography 54 (4), 1257–1271.

Eisner, L.B., Twardowski, M.S., Cowles, T.J., Perry, M.J., 2003. Resolving phytoplankton photoprotective: photosynthetic carotenoid ratios on fine scales using in situ spectral absorption measurements. Limnology and Oceanography 48, 632–646.

Eleveld, M., Pasterkamp, R., Van Der Woerd, H., Pietrzak, J., 2008. Remotely sensed seasonality in the spatial distribution of sea-surface suspended particulate matter in the southern North Sea. Estuar. Coast. Shelf Science 80, 103–113.

Falkowski, P., 1994. The role of phytoplankton photosynthesis in global biogeochemical cycles. Photosynthesis Research 39, 235–258.

Ferrari, G., Tassan, S., 1999. A method using chemical oxidation to remove light absorption by phytoplankton pigments. Journal of Phycology 35, 1090–1098.

Fettweis, M., Van Den Eynde, D., 2003. The mud deposits and the high turbidity in the Belgian–Dutch coastal zone Southern Bight of the North Sea. Continental Shelf Research. 23, 669–691.

Gons, H.J., Rijkeboer, M., Ruddick, K., 2002. A chlorophyll-retrieval algorithm for satellite imagery (Medium Resolution Imaging Spectrometer) of inland and coastal waters. Journal of Plankton Research 24, 947–951.

Hoepffner, N., Sathyendranath, S., 1991. Effect of pigment composition on absorption properties of phytoplankton. Marine Ecology Progress Series 73, 11–23.

Jonasz, M., 1983. Particle size distribution in the Baltic. Tellus Series B 35, 346–358.

Jonasz, M., 1987. Nonspherical sediment particles: Comparison of size and volume distributions obtained with an optical and resistive particle counter. Marine Geology 78, 137–142.

Kirk, J.T.O., 1994. Light and Photosynthesis in Aquatic Ecosystems. Cambridge University Press, Cambridge.

Lancelot, C., Billen, G., Sournia, A., Weisse, T., Colijn, F., Veldhuis, M.J.W., Davies, A., Wassman, P., 1987. *Phaeocystis* blooms and nutrient enrichment in the continental coastal zones of the North Sea. Ambio 16, 38–46.

Lancelot, C., 1995. The mucilage phenomenon in the continental coastal waters of the North Sea. Science of the Total Environment 165, 83–102.

Lorenzen, C.J., Jeffrey, S.W., 1980. Determination of chlorophyll in seawater. UNESCO. Tech. Pap. Mar. Sci. 35, 20.

Leymarie, E., Doxaran, D., Babin, M., 2010. Uncertainties associated to measurements of inherent optical properties in natural waters. Applied Optics 49, 5415–5436.

Lubac, B., Loisel, H., 2007. Variability and classification of remote sensing reflectance spectra in the eastern English Channel and southern North sea. Remote Sensing of Environment 110, 45–58.

Morel, A., 1973. Light scattering by seawater. Experimental results and theoretical approach., in: Optics of the sea. AGARD Lect. Ser., NATO, Neuilly-sur-Seine, pp. 3.1.1–3.1.76.

Nechad, B., Ruddick, K., Park, Y., 2010. Calibration and validation of a generic multisensor algorithm for mapping of total suspended matter in turbid waters. Remote Sensing of Environment 114, 854–866.

Pegau, W.S., Deric, G., Zaneveld, J.R.V., 1997. Absorption and attenuation of visible and near-infrared light in water: Dependence on temperature and salinity. Applied Optics 36, 6035–6046.

Peters, S.W.M., Eleveld, M.A., Pasterkamp, R., van der Woerd, H.J., Devolder, M., Jans, S., Park, Y., Ruddick, K., Block, T., Brockmann, C., Doerffer, R., Kraseman, H.L., Röttgers, R., Schönfeld, W., Jørgensen, P.V., Tilstone, G.H., Martinez-Vicente, V., Moore, G.F., Sørensen, K., Høkedal, J., Johnsen, T.M., Lømsland, E.R., Aas, E., 2005. Atlas of Chlorophyll-a Concentration for the North Sea based on MERIS Imagery of 2003. Vrije Universiteit Amsterdam, The Netherlands.

Reynolds, R.A., Stramski, D., Wright, V.M., Wozniak, S.B., 2010. Measurements and characterization of particle size distributions in coastal waters. Journal of Geophysical Research, 115. doi:10.1029/2009JC005930.

Risovic, D., 1993. Two component model of sea particle size distribution. Deep Sea Research, Part I 40, 1459–1473.

Rousseau, V., Park, Y., Ruddick, K., Vyverman, W., Parent, J.-Y., Lancelot, C., 2006. Phytoplankton blooms in response to nutrient enrichment. In: Rousseau, V., Lancelot, C., Cox, D. (Eds.), Current Status of Eutrophication in the Belgian Coastal Zone. Presses Universitaires de Bruxelles, Brussels, pp. 45–59.

Rousseau, V., Chrétiennot-Dinet, M.-J., Jacobsen, A., Verity, P., Whipple, S., 2007. The life cycle of Phaeocystis: state of knowledge and presumptive role in ecology. Biogeochemistry 83, 29–47.

Ruddick, K.G., Gons, H.J., Rijkeboer, M., Tilstone, G., 2001. Optical remote sensing of chlorophyll a in Case 2 waters by use of an adaptive two-band algorithm with optimal error properties. Applied Optics 40, 3575–3585.

Ruddick, K., Lacroix, G., 2006. Hydrodynamics and meteorology of the Belgian Coastal Zone. In: Rousseau, V., Lancelot, C., Cox, D. (Eds.), Current Status of Eutrophication in the Belgian Coastal Zone. Presses Universitaires de Bruxelles, Brussels, pp. 1–16.

Schiller, H., Doerffer, R., 1999. Neural network for emulation of an inverse model—operational derivation of Case II water properties from MERIS data. International journal of remote sensing 20, 1735–1746.

Snyder, W., Arnone, R., Davis, C., Goode, W., Gould, R., Ladner, S., 2008. Optical scattering and backscattering by organic and inorganic particulates in US coastal waters. Applied Optics 47, 666–677.

Sullivan, J.M., Twardowski, M.S., Donaghay, P.L., Freeman, S.A., 2005. Use of optical scattering to discriminate particle types in coastal waters. Applied Optics 44, 1667–1680.

Tassan, S., Ferrari, G., 1995. An alternative approach to absorption measurements of aquatic particles retained on filters. Limnology and Oceanography 40, 1358–1368.

Tassan, S., Ferrari, G., 1998. Measurement of light absorption by aquatic particles retained on filters: determination of the optical pathlength amplification by the 'transmittance–reflectance' method. Journal of Plankton Research 20, 1699–1709.

Tassan, S., Ferrari, G.M., 2002. A sensitivity analysis of the 'Transmittance–Reflectance' method for measuring light absorption by aquatic particles. Journal of Plankton Research 24, 757–774.

Williams, P.J.L., Thomas, D.N., Reynolds, C.S., 2002. Phytoplankton productivity: Carbon assimilation in marine and freshwater ecosystems. Blackwell Science, U.K.

Zaneveld, J.R.V., Bartz, R., Moore, C.M., 1994. The scattering error correction of reflecting-tube absorption meters. Proceedings SPIE, Ocean Optics XII. 2258, pp. 44–55.